

# **Analogue Optical Links for the CMS Tracker Readout System**

Presented by V. Arbet-Engels

V. Arbet-Engels, G. Cervelli, K. Gill, R. Grabit, C. Mommaert, G. Stefanini, and F. Vasey  
CERN, CH - 1211 Geneve 23, Switzerland

## **Abstract**

Fibre optic links are being developed for analogue signal transfer from the front-end electronics of the tracker in the CMS experiment at the CERN Large Hadron Collider (LHC). The links are based on the direct modulation of edge-emitting lasers located inside the detector volume. The optical signals are transmitted over single mode optical fibres to the counting room and detected using PIN photodiodes. Results recently obtained with a one-channel link demonstrator are reported. The overall performance is discussed in terms of static and dynamic responses.

Corresponding author:

Vincent Arbet-Engels  
CERN, ECP Division  
CH 1211 Geneva 23  
Switzerland  
tel: +41 22 767-8583  
fax: +41 22 767-2800  
email: [vincent.arbet.engels@cern.ch](mailto:vincent.arbet.engels@cern.ch)

## 1. Introduction

The CMS central tracker consists of silicon and gas microstrips with an inner pixel detector system. The total number of microstrip detector channels is  $12 \cdot 10^6$ . The electronic readout scheme envisaged for all microstrip detectors is based on a front-end chip with analogue pipelines [1]. Following a level 1 trigger, the corresponding analogue samples are time multiplexed and transmitted over optical fibre links to the digitizers in the counting room. One optical fibre carries signals from 256 detector channels. Thus, the readout of the microstrip detectors requires over 50,000 analogue fibre links. The link requirements are reviewed and the results obtained with a one-channel link demonstrator are reported.

## 2 Overview of the system

The silicon and gas microstrip are read out by charge sensitive amplifiers whose voltages are sampled at the beam crossing rate of 40 MHz. The samples are stored in analogue pipelines of the front-end APV chip [2] during the level 1 trigger latency and, following a trigger, are time-multiplexed at a rate of 40 MSamples/s into the analogue optical fibre links and transmitted to the digitizers (FED modules) in the counting room, where they are converted back to electrical signals by PIN photodiode receivers. The length of the fibres is 150 m. A more detailed description of the read-out chain can be found elsewhere [3].

The main requirements on the link performance can be summarized as follows: (a) full scale dynamic range 200:1, with <2% deviation from linearity, and (b) overall link noise contribution (rms) equivalent to < 0.2% of full scale.

These requirements may not seem outstanding in view of current standards, but it should be stressed that they must be achieved and maintained in the challenging front-end environment, where the devices will be subjected to very high radiation levels. The integrated dose and hadronic fluence in the tracker volume are estimated to 10 MRad and  $10^{14}$  (1Mev neutron equivalent)/ $\text{cm}^2$ , respectively, over the projected 10 years of operation [4]. Other technical constraints on the front-end components include low power dissipation, low mass, operation in a magnetic field of up to 4T, and very limited accessibility for servicing [5]. The various constraints raise unprecedented challenges in the reliability of the components and systems, in particular of the optical link transmitters, under the specific operating conditions.

The analogue optical link described in this paper is the final outcome of a development program of several years, during which several technologies have been investigated. The transmitters are directly modulated, edge-emitting laser diodes. The lasing wavelength is 1.3  $\mu\text{m}$  (2nd telecom window) and the optical fibres are single-mode, pure-silica core. The main criteria driving the technical choices are optimal performance, availability, and cost; the optoelectronic devices and the fibres are commercial products, whose decreasing cost trend is

driven by volume applications in the telecom and datacom market. A major effort has been made in validating the technologies for radiation hardness and in developing specific packages. The effects of gamma and neutron irradiations on laser diodes and optical fibres are the subject of an ongoing study [6,7]. The results obtained so far indicate very good radiation hardness; a model to estimate the resulting consequences on link performance under realistic operating conditions is being developed.

### 3. Link demonstrator

A one-channel link demonstrator, schematically shown in Fig. 1, has been built and tested. The optoelectronic devices are commercially available products, of the same type as the ones intended for the final system. The laser driver and photodiode amplifier are built from off-the-shelf discrete components (a driver ASIC in full rad-hard technology is being presently designed). In the following sections, the transmitter and the receiver modules are described and the full link characteristics are discussed.

#### 3.1 Analogue transmitter

The analogue transmitter consists of a multiple quantum well Fabry-Perot InGaAsP edge emitting laser [8] directly modulated by a transconductance amplifier. The laser emission wavelength occurs at 1.3  $\mu\text{m}$  from band to band transitions in the strained quantum wells. A typical laser L-I curve is shown in Fig. 2. The two important extracted parameters are the threshold current,  $I_{\text{th}}$ , and the slope efficiency, ( $\eta = dP_{\text{laser}}/dI_{\text{laser}}$ ). The threshold current sets the limit above which stimulated emission builds up at the expense of the non-coherent spontaneous emission and optical gain balances the total losses. The slope efficiency specifies the amount of output light power per injected drive current above threshold. The investigated lasers have a typical threshold current close to 8 mA and slope efficiency 0.2 W/A. The laser die and fibre are actively aligned to each other and bonded onto a common Si-submount with footprint dimensions 2x2x1 mm. The resulting compact and low mass sub-assembly is further encapsulated into a mini-DIL ceramic package.

The driver provides the dc pre-bias as well as the modulation current, proportional to the input voltage signal  $V_{\text{in}}$ . The pre-bias working point, shown in Fig. 2, is set by adjusting a reference input resistor of a monolithic dual transistor current mirror. The modulation current is controlled by a wide bandwidth operational transconductance amplifier. The static characteristic of the laser driver is shown in Fig. 3 for three different pre-bias conditions, 4 mA, 10 mA, and 20 mA, respectively. The measured transconductance,  $G_m$ , is 5.2 mA/V and is independent of the DC bias point. Hence, multiplying  $G_m$  by the laser slope efficiency  $\eta$ , the transmitter gain

is calculated to be 1.14  $\mu\text{W}/\text{mV}$ . The time delay with the present transmitter configuration is 1.8 ns.

### 3.2 Analogue receiver

The analogue receiver module consists of a reverse biased PIN photodiode and a transimpedance amplifier. In the final readout system, the voltage output of the amplifier will be connected to the input of the ADC converter on the FED board. The back illuminated photodiode consists of a lattice matched InGaAs active layer grown on top of a transparent InP substrate. It produces a photocurrent proportional to the incoming light. The factor of proportionality corresponds the photodiode responsivity,  $R_{\text{PIN}}$ , and is 0.96 A/W for the present diodes. The fibre light is coupled to the photodiode through the use of an angle etched Si-submount onto which both fibre and diode are attached. The assembling scheme is similar to the transmitter module with a small footprint Si-submount housed in a mini-DIL package.

The photodiode is dc-coupled to the amplifier. The use of a dc-coupled receiver permits the on-line monitoring of the quasi-static link performance. A compensation network allows to adapt the receiver operating range to the DC bias point. The transimpedance amplifier, built from discrete IC's mounted onto a small printed circuit board, has a gain resistor,  $R_{\text{RX}}$ , equal to 9.93 K $\Omega$ . The receiver static response is shown in Fig. 4 where the photocurrent,  $I_{\text{pin}}$ , has been converted to an optical power,  $P_{\text{pin}}$ , using  $P_{\text{pin}} = I_{\text{pin}}/R_{\text{PIN}}$ . The full receiver responsivity is then measured to be 9.53 mV/ $\mu\text{W}$ . The receiver saturates at 3.6 V, corresponding to a maximum injected optical power of 400  $\mu\text{W}$  above the laser dc power. The measured receiver overall time delay is 3.3 ns.

### 3.3 Full link characteristic

The link gain is expressed as follows:

$$\frac{V_{\text{OUT}}}{V_{\text{IN}}} = R_{\text{RX}} \times R_{\text{PIN}} \times \eta \times G_{\text{m}} \times \text{IL}_{\text{connector}}$$

where  $R_{\text{RX}}$  is the receiver transresistance,  $R_{\text{PIN}}$  the photodiode responsivity,  $\eta$  the laser slope efficiency,  $G_{\text{m}}$  the laser driver transconductance, and  $\text{IL}_{\text{connector}}$  the connector insertion losses. The transmitter and receiver fibre pigtailed were linked using a FC-PC optical connector with an average insertion loss, IL, of 0.2 dB. The static response of the full link was measured at room temperature with a stabilized voltage source and is shown in Fig. 5. The laser and PIN diode were not temperature controlled. The hatched pattern represents the operating quadrant for ADC signals ranging between 0 and 3V and injected signal levels between 0 and 300 mV. The experimental average link gain is 10.9, in close agreement with the 10.3 gain value

computed from the independent link component characteristics using the above expression. The calculated relative distortion with respect to a linear fit is  $<2\%$  for input signals in the range of  $\pm 300$  mV.

The link demonstrator step response is shown in Fig. 6a. The straight line refers to the input signal with the scale on the left axis. The dotted line represents the output signal and is plotted against the right axis. The input signal is typical of the signal to be delivered by the front-end APV chip with a rise time of 5ns and a plateau of 20ns. We measure an overshoot of  $\approx 20\%$  of the pulse height and a settling time of 15ns to within 1% of the end value. It is worth recalling that signals will be digitized within the 25ns of the sample period.

The full link frequency response is shown in Fig. 6b, where measured points are compared to a line fit based on a second order filter analytical model. The static link gain is 15.1 dB (into 50  $\Omega$ ) and is consistent with the dc gain value mentioned above. By applying an inverse Fourier transformation on the fit, the temporal step response was synthesized and the measured 15ns settling time value was confirmed. The -3dB cut-off frequency happens at 172 MHz and is mostly limited by the receiver bandwidth. Also, a +3dB resonance peak is observed at around 90 MHz. It produces detrimental ringing in the time domain and work is in progress to increase the damping and better compensate the system response.

In the 172 MHz link bandwidth of this link prototype, the equivalent input noise is  $\approx 10$  mV and the peak signal to noise ratio (SNR)  $\approx 300/1$ . The corresponding equivalent noise charge (ENC) for the front-end system is  $\approx 1300 e^-$ . The main sources of noise are the thermal or Johnson noise of the electronics, the intensity (laser RIN) or phase fluctuations inherent to the lasing action, and phase to intensity noise generated by interferometric cavities from interfaces along the link. Indeed, it was found that the noise level is highly sensitive to the quality of the optical connections. Nevertheless, the SNR can easily be improved by decreasing the system bandwidth. A reduction by a factor of two should theoretically augment the SNR by  $\approx 2$  and a preliminary study has shown that limiting the bandwidth using a first order filter will not degrade the settling time significantly [9].

## 4 Conclusion

An analogue optical fibre link based on commercially available optoelectronic devices is being developed for the CMS tracker readout system. Its conception takes full advantage of today's mature lightwave technology and will benefit from the trend to lower cost of the volume telecom applications. A prototype link demonstrator has been built and fully characterized. The reported performance meets all the requirements for the electronic readout of the tracker. The radiation hardness of the devices has been validated and further studies are in progress. The development of 4-way links with laser driver ASICs in rad-hard technology is under way.

## References

- [1] G. Hall and G. Stefanini, CMS TN/94-137
- [2] MDM de Fez-Laso et al., Nucl. Inst. and Meth. A382, 533 (1996)
- [3] G. Hall, Nucl. Inst. and Meth. A386, 138 (1997)
- [4] The Compact Muon Solenoid Technical Proposal. CERN Report LHCC 94-38 (1994)
- [5] G. Stefanini, Proceedings of the first workshop on electronics for LHC experiments, Lisbon, 157 (1995)
- [6] K. Gill et al., to be published in J. Non-Cryst. Solids (1997)
- [7] K. Gill et al., CMS Note 044 (1997)
- [8] G. P. Agrawal and N. K. Dutta, Semiconductor Lasers (Van Nostrand Reinhold, New York, 1993)
- [9] G. Cervelli, private communication

## Figure captions

- Fig. 1 Schematic of the analogue link with the transmitter and the receiver modules.
- Fig. 2 Typical L-I curve of a semiconductor laser indicating the threshold current, the dc bias point, and the slope efficiency.
- Fig. 3 Static characteristic of the laser driver for three different bias conditions, 4 mA, 10 mA and 20 mA, respectively.
- Fig. 4 Analogue receiver static characteristic.
- Fig. 5 Full link transfer characteristic. The upper right quadrant (hatched pattern) corresponds to the 0-3 V operating range of the ADC.
- Fig. 6a Full link step response to a representative APV signal.
- Fig. 6b Frequency spectrum of the full link response. The dots are the experimental data and the line a fit using a second order filter analytical model.

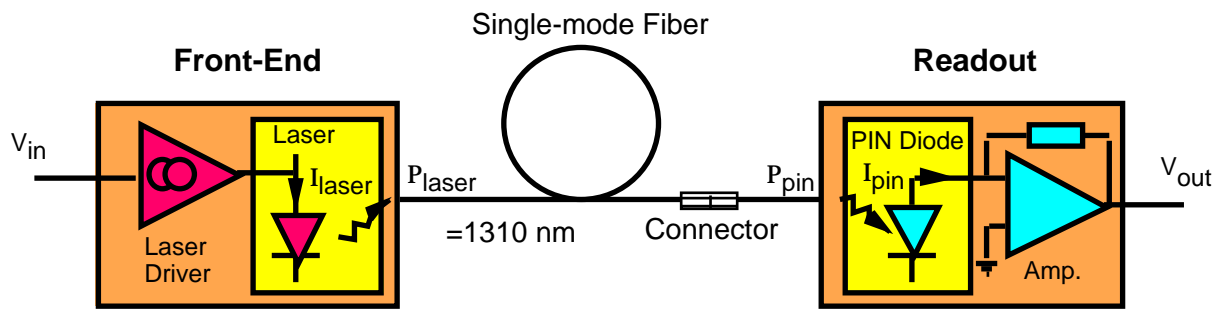


Fig. 1

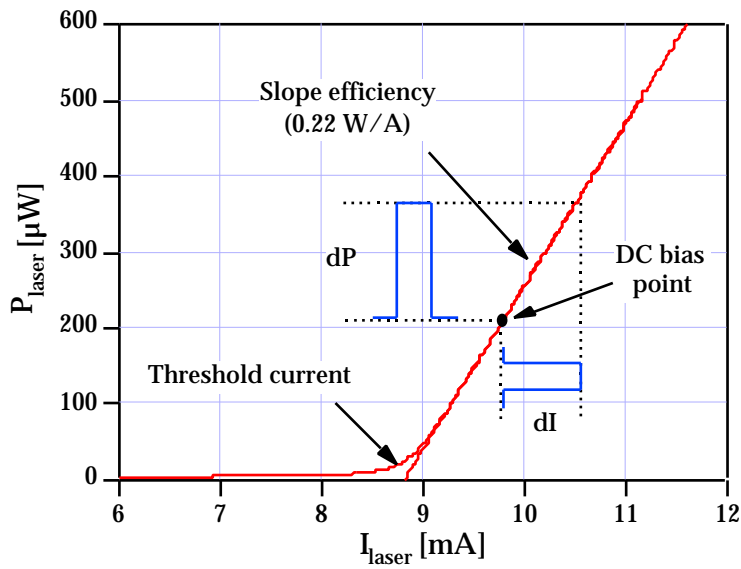


Fig. 2

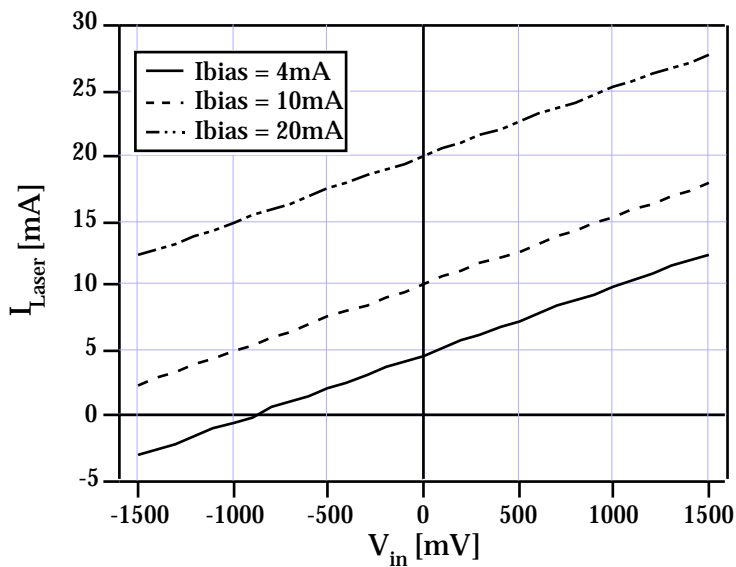


Fig. 3



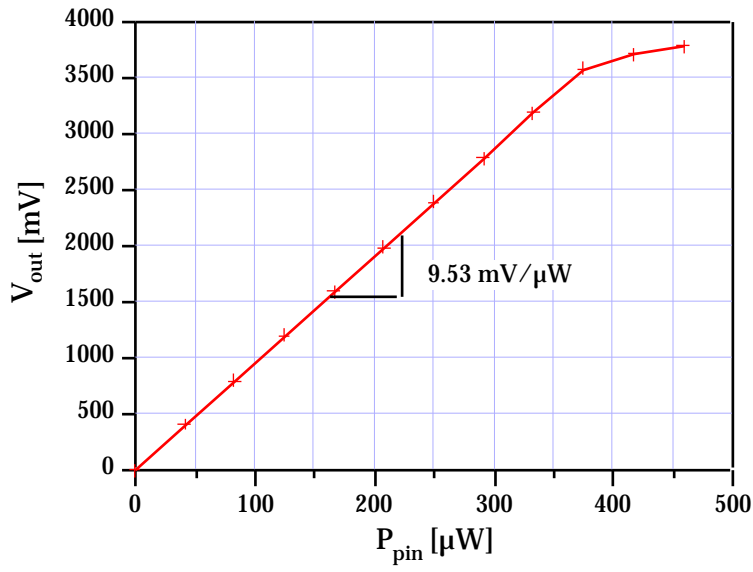


Fig. 4

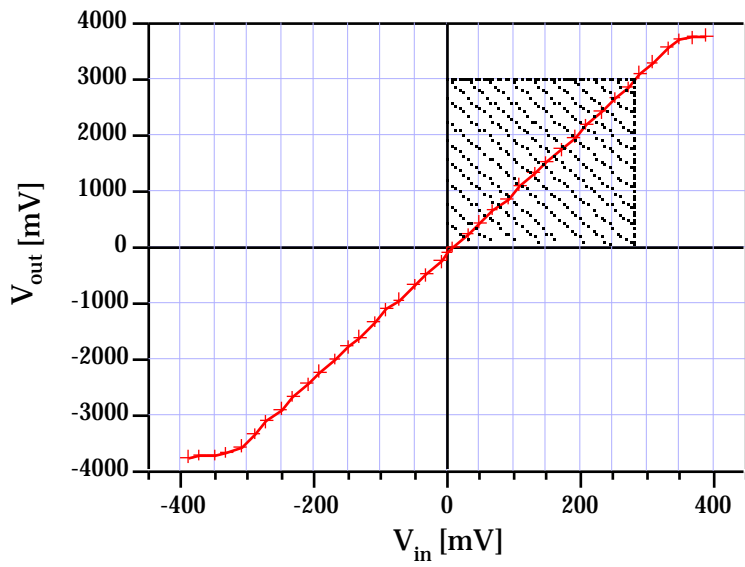


Fig. 5

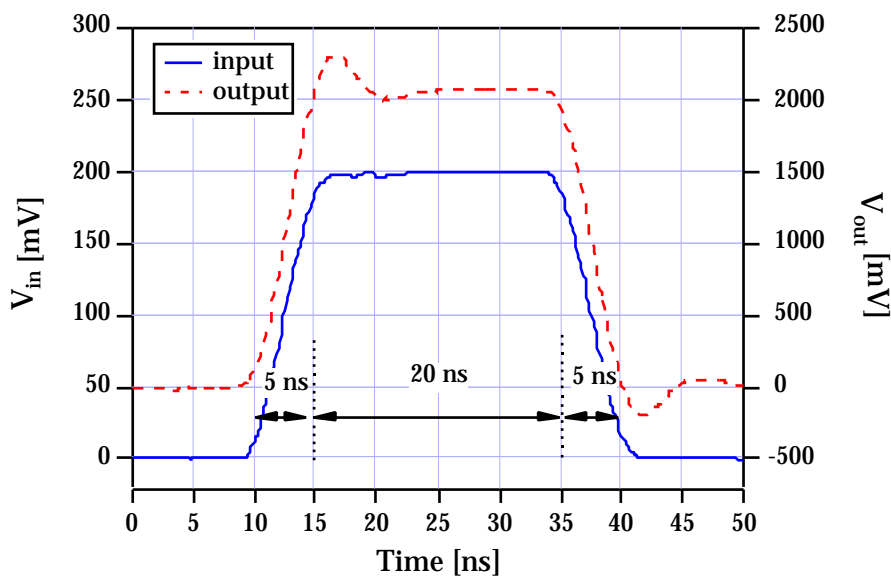


Fig. 6a

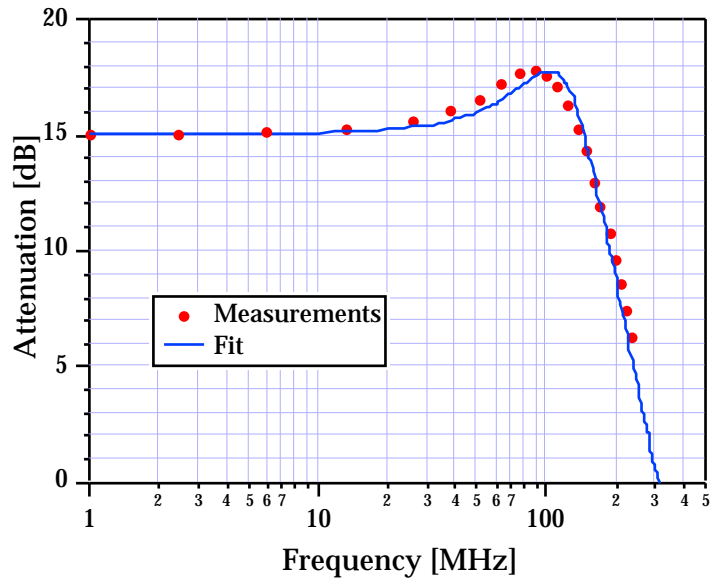


Fig. 6b